Research and Reviews in Materials Science and Chemistry
Vol. 5, Issue 2, 2015, Pages 93-113
ISSN 2319-6920
Published Online on September 15, 2015

http://jyotiacademicpress.net

ON THE THERMAL CONDUCTIVITY OF $CoSi/Al_2O_3$ NANOCOMPOSITES

MARIA IOANNOU and THEODORA KYRATSI

Department of Mechanical and Manufacturing Engineering
University of Cyprus
1678 Nicosia
Cyprus
e-mail: kyratsi@ucy.ac.cy

Abstract

In this work, the development of nanocomposites through the introduction of Al_2O_3 nanoparticles into the matrix of CoSi is presented. CoSi was prepared through solid state reaction and different concentrations of nano-Al_2O_3, were introduced by mechanical grinding. The nanocomposites were fabricated via hot pressing and studied in terms of Seebeck coefficient, electrical and thermal conductivities at temperature range of 300-950K. Special emphasis was given to the reduction of the lattice thermal conductivity of nanocomposites and a comparative analysis with the effective medium theory was done to study the effect of nano-Al_2O_3, as well as porosity of the CoSi matrix.

1. Introduction

Most energy resources are discharged as waste heat into the environment without practical applications. Industrial processes, automotive exhaust, and home heating generate waste heat that could be converted to electricity by using thermoelectric applications. The

Keywords and phrases: intermetallic compounds, thermoelectric materials, hot press, porosity.
Communicated by Emad M. El-Menyawy.
Received June 17, 2015; Revised July 16, 2015

successful commercial exploitation of thermoelectric devices depends on increasing the material's figure of merit, which comprises three key transport parameters, i.e., the Seebeck coefficient (S), the electrical conductivity (σ), and the thermal conductivity (κ) along with the absolute temperature T given by the expression: $ZT = S^2\sigma T/\kappa$. It is noteworthy that significant advance in ZT has been made by nanocomposite approach, but still not good enough for broad range of applications.

CoSi has been reported to be one promising candidate for advanced thermoelectrics [1-3]. It has the CsCl structure [4], and shows very low electrical resistivity ($\sim 10^{-4}\Omega$cm) but quite large Seebeck coefficient at room temperature [5, 6], therefore, it exhibits a relatively high room-temperature thermoelectric power factor ($\sim 5\text{mWK}^{-2}\text{m}^{-1}$). This value is comparable to that of state-of-the-art Bi_2Te_3 materials ($\sim 4\text{mWK}^{-2}\text{m}^{-1}$) [7], however, the thermal conductivity of CoSi is too high resulting low ZT.

The reduction of the thermal conductivity can be attained by nanostructuring of bulk materials. The nanostructures introduce complexity by additional phonon scattering mechanisms through materials engineering. TE nanocomposites, produced by adding nano-inclusions or mixing nanostructured phases, have been reported [8-12] to exhibit increased phonon scattering [13-16] making their lattice thermal conductivity much lower compared to that of their equivalent large crystalline bulk materials.

In previous works, we attempted to improve the thermoelectric properties of CoSi by successfully decreasing thermal conductivity the development of nanocomposites (with SiO_2 [17]). In this work, the reduction of the thermal conductivity using a different oxide (nano-Al_2O_3) is attempted. The $CoSi/Al_2O_3$ nanocomposites were studied in terms of structural and morphological characteristics, while the thermoelectric properties are also presented. Finally, the reduction of the lattice thermal conductivity via formation of nanocomposite materials is discussed in the view of the effective medium theory.

2. Materials and Methods

The aim was to develop composite materials consisting of (a) matrix with structural features of the order of micrometers and (b) dispersed phase with structural features of the order of nanometers. Therefore, cobalt and silicon powders were (a) grinded inside mortar, in order to have mixed and fine powders, (b) cold-pressed and heated, in order to get the pure single phase cobalt silicide through solid state reaction, (c) mixed with the nano-Al_2O_3 by mechanical grinding, and finally (d) hot-pressed for the formation of nanocomposites, in order to study the modifications in the thermoelectric properties.

2.1. Reagents

Chemicals in this work were used as obtained: (i) Cobalt powder (− 22mesh [= 622μm], 99.9988% purity, Alfa Aesar); (ii) Silicon powder (crystalline, +100mesh [= 149μm], 99.9% purity, Alfa Aesar), and (iii) Aluminum oxide (Al_2O_3) nanopowder (< 50nm, Sigma-Aldrich). All manipulations were carried out under inert gas argon in a dry glove box.

2.2. Grinding and heating treatment

The Co and Si powders were mixed in the appropriate ratio (1:1), cold-pressed to pellets and heated at 1000°C for 20hrs under vacuum, as presented in more detail elsewhere [17].

The prepared CoSi powders were mixed with nano-Al_2O_3 following:

$$(1 - x)\mathrm{CoSi} + x\ \mathrm{Al_2O_3}, \tag{1}$$

with x values 0.0%, 1.0%, 2.5%, 5.0%, 7.5%, 10%, and 15% (referred in text as $\mathrm{CoSi}/x\ \mathrm{Al_2O_3}$). After $\mathrm{CoSi}/x\ \mathrm{Al_2O_3}$ mixing, the powders were sintered in a uni-axial hot-press system (HP20 from Thermal Technologies Inc.) at 1000°C for 60min under 80MPa and argon flow, in order to perform thermoelectric measurements. The hot-pressed pellets

had densities between 5.18 to 6.25g/cm^3. The density of the pellets was estimated from mass (m) and volume (V) measurements using the equation

$$\rho_{meas} = m / V. \quad (2)$$

2.3. Structural characterization and elemental analysis

Powder X-ray diffraction (PXRD) patterns were obtained on all materials, using a Rigaku Miniflex system with Ni-filtered Cu Ka radiations (30kV, 15mA) in order to identify the phases and evaluate purity of the products. The morphological characterization of the powders was carried out by scanning electron microscopy (SEM) (Tescan Vega LSU as well as Jeol 840A). Jeol 840A scanning microscope with an energy dispersive spectrometer attached (Oxford, model ISIS 300) was used for energy dispersive X-ray analysis (EDX) and the elemental distribution images on polished surfaces.

2.4. Thermoelectric properties

Thermal conductivity. A Netzsch LFA-457 system was used to measure thermal diffusivity and heat capacity of the hot-pressed pellets. The thermal conductivity was calculated from the experimental thermal diffusivity (α) and a specific heat capacity data (C_p), as well as density values (ρ), based on the equation $\kappa = \alpha \times \rho \times C_p$. The C_p values were obtained from measurements using the same laser flash system and pyroceramic material as reference.

Seebeck coefficient and electrical conductivity. The measurements were carried out on the hot-pressed pellets simultaneously using a commercial ZEM-3 Seebeck coefficient and electrical resistivity measurement system from ULVAC-RIKO. Data were recorded in the temperature range of room temperature to 973K. The measurements were performed under a residual pressure of helium gas to facilitate good thermal contact.

3. Results and Discussion

3.1. Consolidation and structural characterization

PXRD shows that CoSi is the only existing phase in the starting powders, see Figure 1, as discussed elsewhere [19]. Interestingly, after CoSi and Al_2O_3 mixing for the formation of $CoSi/x\,Al_2O_3$ nanocomposites and hot pressing, the PXRD patterns are identical with that in the Figure 1 and no traces of Al_2O_3 were observed. This can be attributed to both, strong fluorescence background of the matrix and low Al_2O_3 concentration.

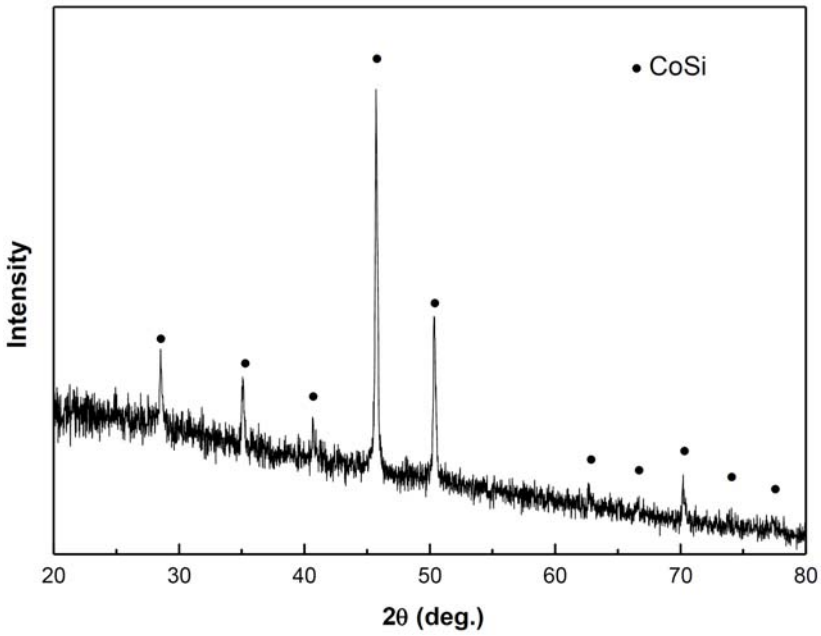

Figure 1. PXRD patterns of CoSi starting powders.

Figure 2 illustrates the density of the hot-pressed $CoSi/x\,Al_2O_3$ nanocomposites pellets as a function of the Al_2O_3 content. The measured density (ρ_{meas}) of the hot-pressed pellets monotonously decreased from $6.25 g/cm^3$ to $5.18 g/cm^3$ with Al_2O_3 concentration up to 15%. It is

noteworthy, that the density of the hot-pressed CoSi matrix corresponds to ~ 95% of the theoretical value for the CoSi. In order to estimate the porosity in the pellets, the theoretical density of the $CoSi/Al_2O_3$ was calculated based on the simple rule of mixtures:

$$\rho_c = f_1\rho_1 + f_2\rho_2,$$

where ρ_c is the theoretical density of the composite and f_1, ρ_1 and f_2, ρ_2 are the volume fraction and the density of the matrix and the Al_2O_3 phase, respectively. Then the porosity in the pellets was estimated following the equation $(\rho_c - \rho_{meas})/\rho_c$, see Table 1. Interestingly, the increased concentration of hard Al_2O_3 makes compaction more difficult and results in higher porosity. Sintering at higher temperatures was attempted but did not improve the density of the pellets.

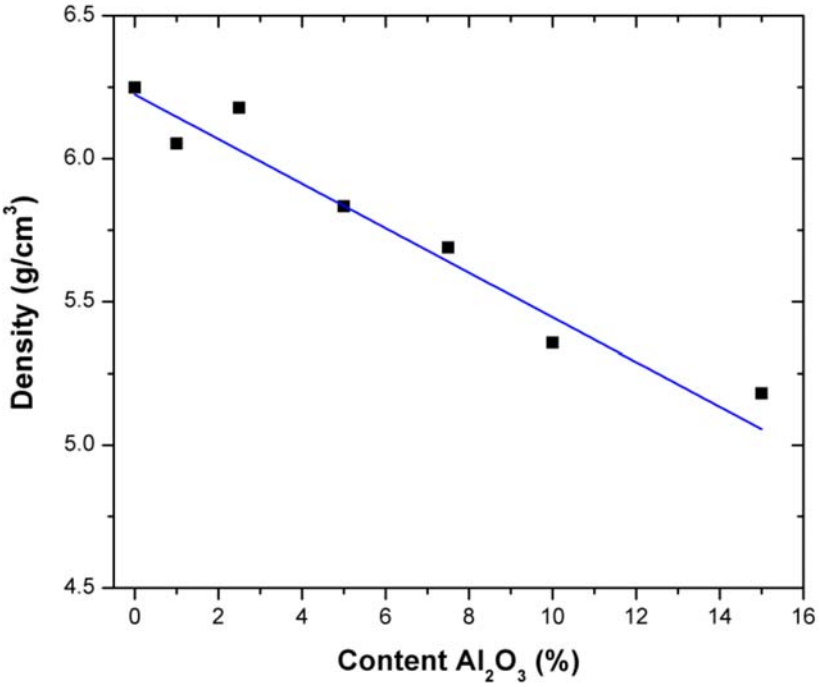

Figure 2. Density of the hot-pressed (1-x) $CoSi/x$ Al_2O_3 nanocomposites pellets as a function of the Al_2O_3 content.

3.2. Scanning electron microscopy and elemental analysis

In order to study the morphology of the CoSi matrix and its nanocomposites, the samples were examined by SEM/EDX. Figures 3(a) and 4(a) show the surface of the CoSi/x Al_2O_3 pellets for x = 7.5% and 15%, where the grain boundaries as well as some porosity were clearly observed in backscattered electron images.

EDX mapping was used to evaluate the distribution of all elements and was carried out for the different elements, i.e., Co, Si, and Al. Figures 3(b)-(d) and 4(b)-(d) show the distribution of Co, Si, and Al on CoSi/7.5% Al_2O_3 and CoSi/15.0% Al_2O_3 pellets, respectively. Based on these results, the distribution of Co and Si was found to be more or less uniform while higher quantity of aluminum was observed on the grain boundaries. This could be attributed to the agglomeration at micro-scale of small amounts of Al_2O_3 on the grain boundaries while they become more evident on the samples with higher nano-Al_2O_3 concentration.

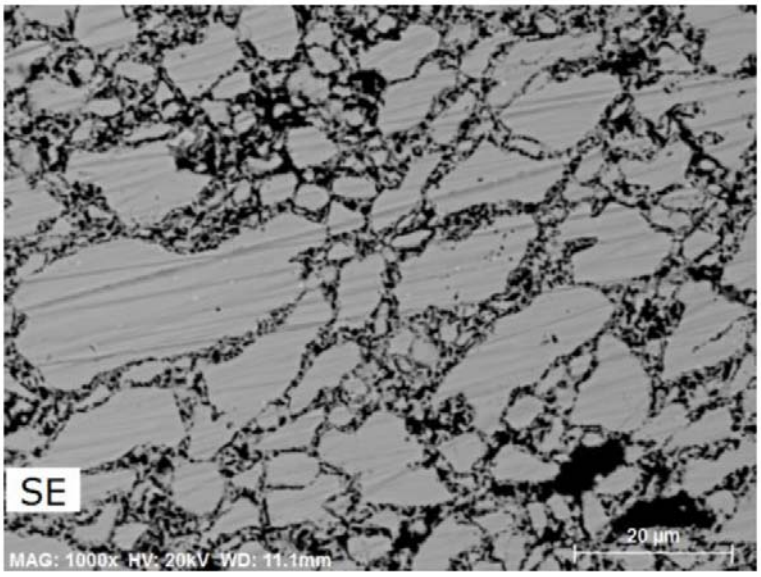
SE
20 µm
MAG: 1000x HV: 20kV WD: 11.1mm

(a)

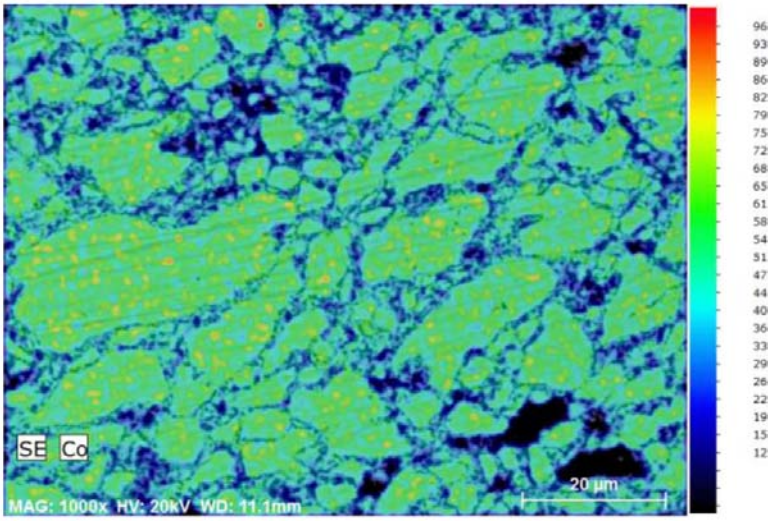
SE Co
20 µm
MAG: 1000x HV: 20kV WD: 11.1mm
96
93
89
86
82
79
75
72
68
65
61
58
54
51
47
44
40
36
33
29
26
22
19
15
12

(b)

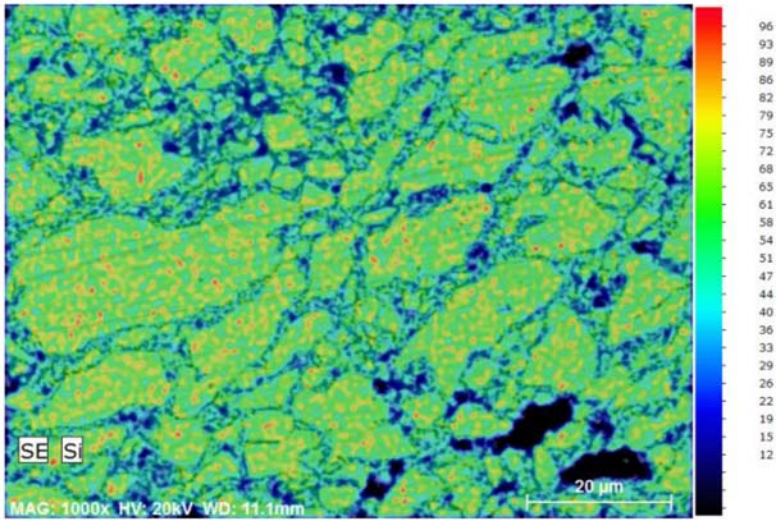

(c)

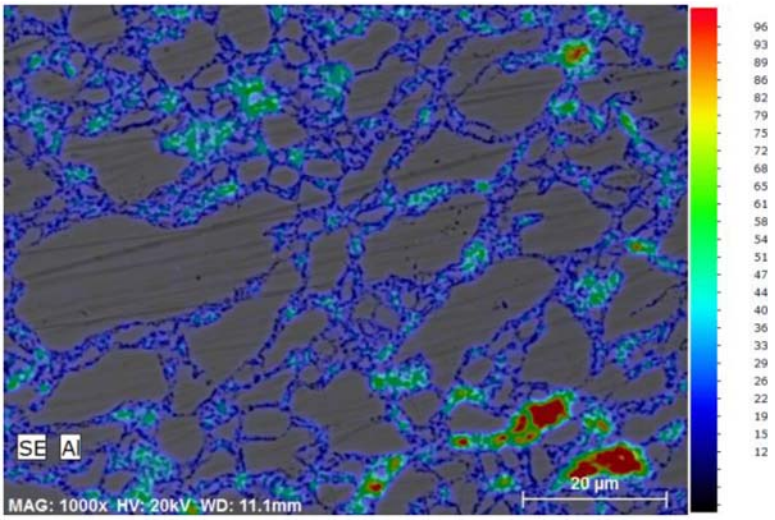

(d)

Figure 3. Backscattered electron (BSE) image (a) and the EDX elemental distribution maps (b)-(d) of Co, Si, and Al, respectively, of the CoSi/7.5% Al_2O_3 nanocomposites. The coloring scheme follows a rainbow scale, from blue (minimum concentration) to red (maximum concentration) and does not correspond to quantitative results.

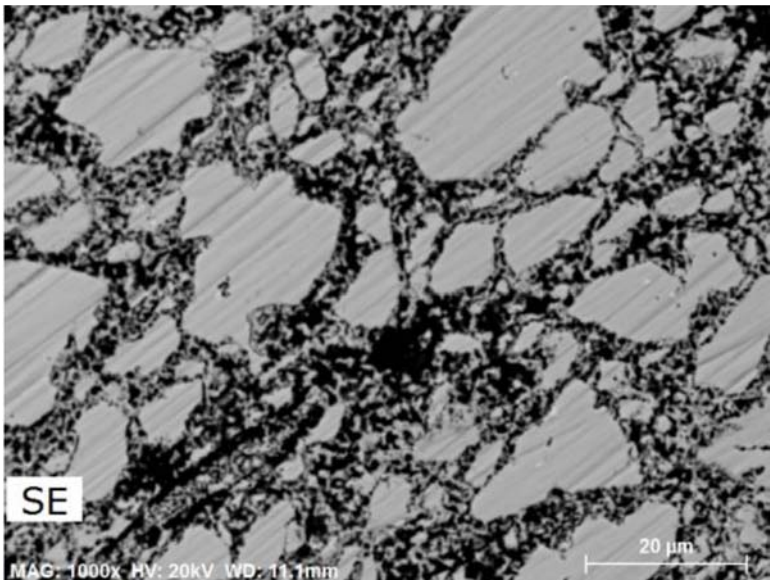
SE
20 µm
MAG: 1000x HV: 20kV WD: 11.1mm

(a)

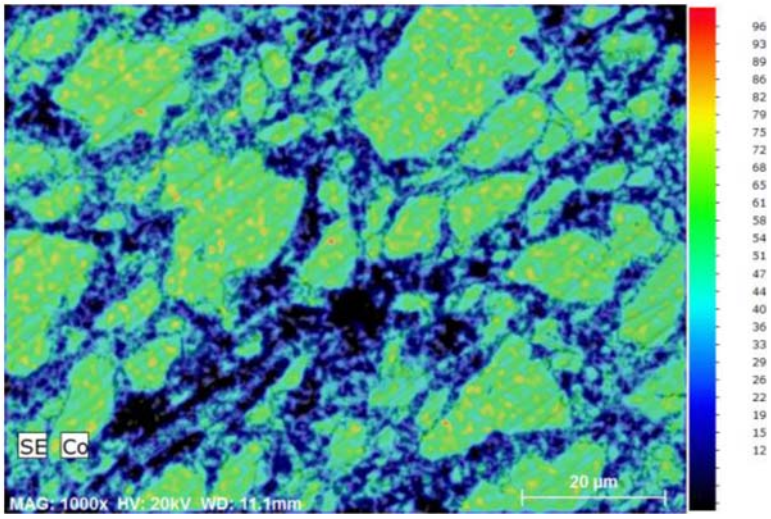
SE Co
20 µm
MAG: 1000x HV: 20kV WD: 11.1mm
96
93
89
86
82
79
75
72
68
65
61
58
54
51
47
44
40
36
33
29
26
22
19
15
12

(b)

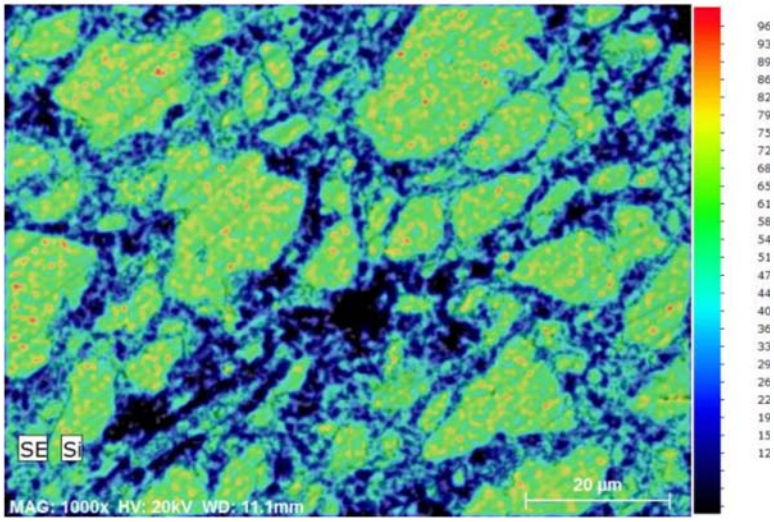

(c)

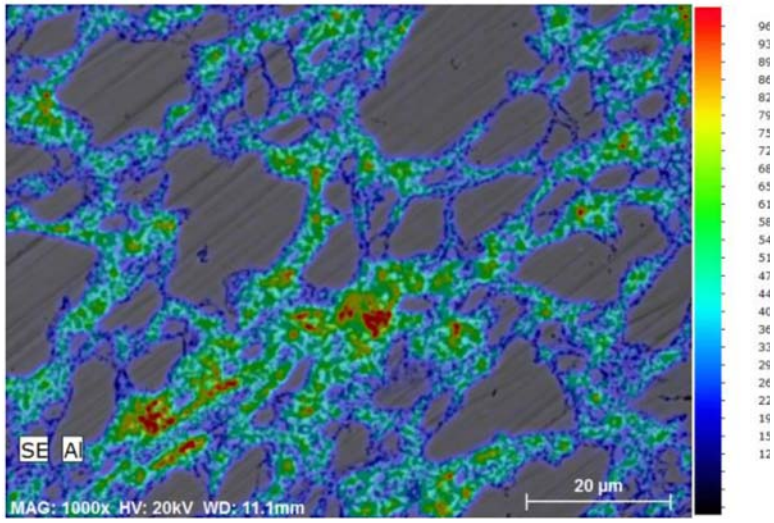

(d)

Figure 4. Backscattered electron (BSE) image (a) and the EDX elemental distribution maps (b)-(d) of Co, Si, and Al, respectively, of the CoSi/15.0% Al_2O_3 nanocomposites. The coloring scheme follows a rainbow scale, from blue (minimum concentration) to red (maximum concentration) and does not correspond to quantitative results.

3.3. Thermoelectric properties

Table 1 lists the results of the measurements (Seebeck coefficient, electrical and thermal conductivity) at 300K for $CoSi/x\ Al_2O_3$ materials. The sign of the Seebeck coefficient of the CoSi matrix and nanocomposites was negative, indicating that the conductivity is mainly due to electrons, as expected. The Seebeck coefficient was found to be similar for all samples, in the range of -80 to $-88\mu V/K$, suggesting similar carrier concentration. In addition, when different Al_2O_3 concentration is introduced, the electrical conductivity significantly drops and this is attributed to lower mobility. The significant effect of the second phase on the reduction of the electrical conductivity can be understood by the contribution of Al_2O_3 aggregates that are formed on the grain boundaries of the materials.

Table 1. Volume fraction of pores and thermoelectric properties of $(1-x)\,\mathrm{CoSi}/x\,\mathrm{Al_2O_3}$ nanocomposites ($0 \le x \le 15\%$) at 300K

Composition	x (%)	Porosity (vol.%)	Electrical conductivity (S/cm)	Seebeck coefficient (μV/K)	Thermal conductivity (W/m·K)	Lattice thermal conductivity (W/m·K)
100.0 CoSi : 0.0 Al_2O_3	0.0	5.0	6178	− 80.7	17.0	12.4
99.0 CoSi : 1.0 Al_2O_3	1.0	7.6	3726	− 83.6	10.8	8.0
97.5 CoSi : 2.5 Al_2O_3	2.5	5.2	3473	− 87.7	10.5	7.9
95.0 CoSi : 5.0 Al_2O_3	5.0	9.5	3321	− 87.9	10.8	8.3
92.5 CoSi : 7.5 Al_2O_3	7.5	10.9	3015	− 83.0	9.6	7.4
90.0 CoSi : 10.0 Al_2O_3	10.0	17.8	2686	− 85.7	10.4	8.4
85.0 CoSi : 15.0 Al_2O_3	15.0	16.2	2093	− 84.1	8.6	7.1

Figure 5 shows the temperature dependence of (a) electrical conductivity, (b) the Seebeck coefficient, (c) thermal conductivity, and (d) lattice thermal conductivity of the $CoSi/x\ Al_2O_3$ ($0 \le x \le 15\%$) hot-pressed pellets. The electrical properties of CoSi indicate semi-metallic behaviour [18-20]. The temperature dependence of the Seebeck coefficient corresponds to the typical behaviour for the CoSi matrix [18-20]. The slope of the electrical conductivity with temperature seems to decrease with Al_2O_3 concentration and this could be attributed to the contribution of Al_2O_3 -phase in mobility.

Figure 5(c) presents the thermal conductivity of $CoSi/x\ Al_2O_3$ nanocomposites ($0 \le x \le 15\%$) as a function of temperature. The room temperature thermal conductivities of $CoSi/x\ Al_2O_3$ nanocomposites decrease from 17W/m·K to 8.6W/m·K when 0.0% and 15.0% Al_2O_3 participates, see Table 1. In order to study the effect of the Al_2O_3 introduction, the lattice thermal conductivity (Figure 5(d)) was estimated based on the Wiedemann-Franz relation $\kappa_L = \kappa - \kappa_e$, where $\kappa_e = L \cdot \sigma \cdot T$ with $L = 2.45 \times 10^{-8} V^2K^{-2}$, using the measured values for thermal (κ) and electrical conductivity (σ). The lattice thermal conductivity of all samples showed a significant decrease when Al_2O_3 was introduced in the material and this can be attributed to the contribution of nano-Al_2O_3 as well as the formation of micro-Al_2O_3 on the grain boundaries (observed by SEM). Interestingly, when the concentration of Al_2O_3 increases, there is no further reduction in lattice thermal conductivity.

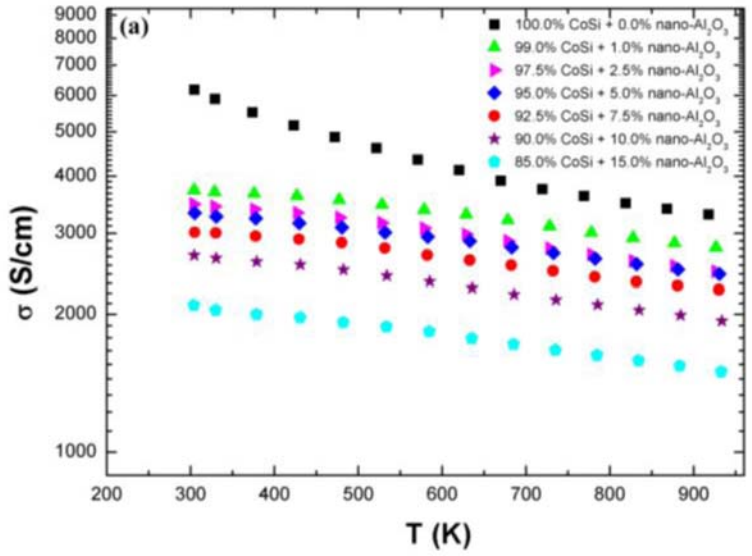
(a)
σ (S/cm)
T (K)
100.0% CoSi + 0.0% nano-Al2O3
99.0% CoSi + 1.0% nano-Al2O3
97.5% CoSi + 2.5% nano-Al2O3
95.0% CoSi + 5.0% nano-Al2O3
92.5% CoSi + 7.5% nano-Al2O3
90.0% CoSi + 10.0% nano-Al2O3
85.0% CoSi + 15.0% nano-Al2O3

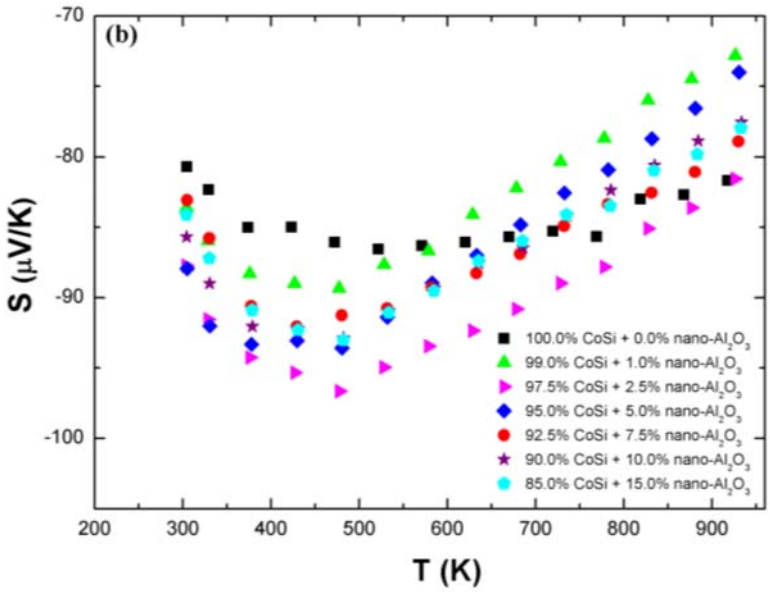
(b)
S (μV/K)
T (K)
100.0% CoSi + 0.0% nano-Al2O3
99.0% CoSi + 1.0% nano-Al2O3
97.5% CoSi + 2.5% nano-Al2O3
95.0% CoSi + 5.0% nano-Al2O3
92.5% CoSi + 7.5% nano-Al2O3
90.0% CoSi + 10.0% nano-Al2O3
85.0% CoSi + 15.0% nano-Al2O3

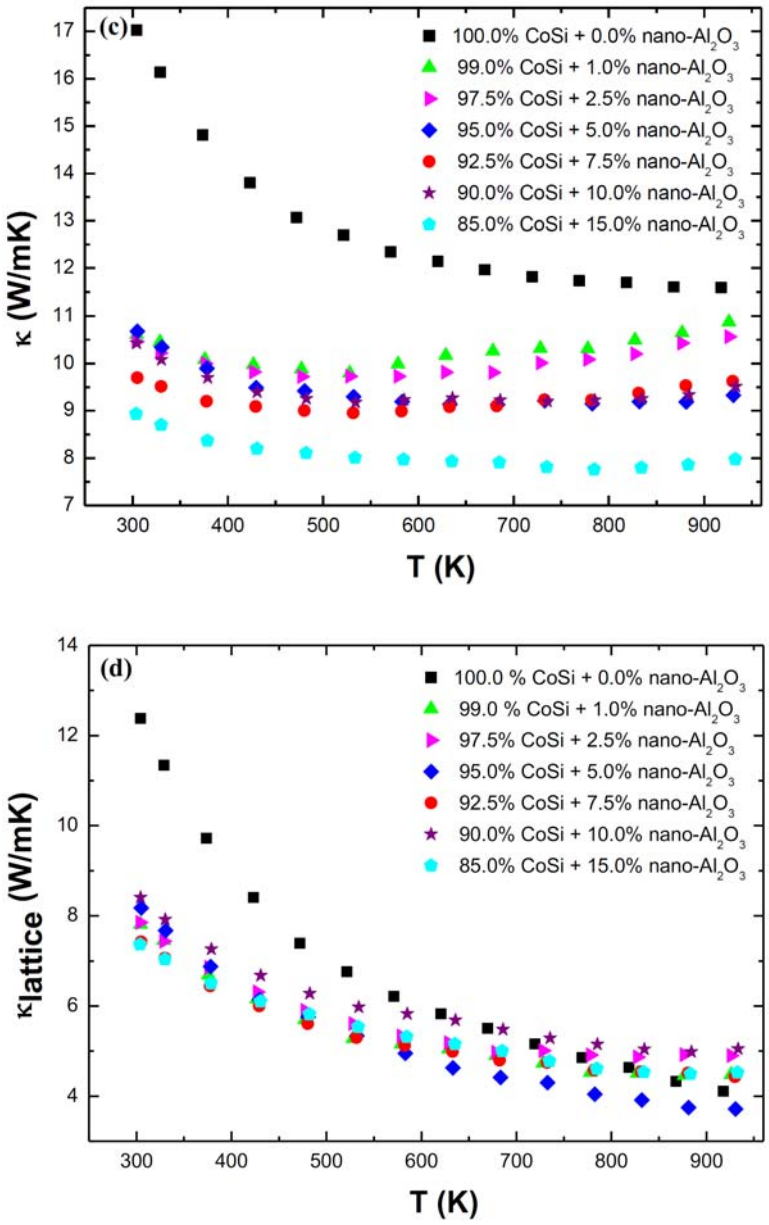

Figure 5. Temperature dependence of electrical conductivity (a); Seebeck coefficient (b); thermal conductivity (c); and lattice thermal conductivity (d) for hot-pressed (1-x) $CoSi/x$ Al_2O_3 nanocomposites pellets.

3.4. Analysis of thermal conductivity

For the analysis of the lattice thermal conductivity, effective medium theory (EMT) was applied to better understand this behaviour using the expression [21, 22]:

$$\sum_i f_i \frac{\kappa_i - \kappa}{\kappa_i + 2\kappa} = 0 \text{ and } \sum_i f_i = 1, \tag{3}$$

where κ_i is the thermal conductivity of the i-th phase with volume fraction f_i. In the first case ($CoSi/Al_2O_3$), the Equation (3) was written in

$$f_1 \frac{\kappa_1 - \kappa}{\kappa_1 + 2\kappa} + f_2 \frac{\kappa_2 - \kappa}{\kappa_2 + 2\kappa} = 0 \text{ and } f_1 + f_2 = 1, \tag{4}$$

where f_1 and f_2 are the fractions of the CoSi matrix phase and the second phase of nano-Al_2O_3, respectively, and κ_1 and κ_2 are the lattice thermal conductivities of the same phases. Taking into consideration the known volume fractions, the thermal conductivity of the matrix ($\kappa_1 = 13.38 W/m{\cdot}K$ as estimated based on the measured porosity of the pellet) and the thermal conductivity of the Al_2O_3 ($\kappa_2 = 16 W/m{\cdot}K$ [23]), Equation (4) is solved numerically for "κ". The results of calculation were shown in the graph with the line labelled "EMT ($CoSi/Al_2O_3$)", in Figure 6. According to the calculations the lattice thermal conductivity was predicted to increase from $13.4 W/m{\cdot}K$ to about $13.8 W/m{\cdot}K$ when 15% Al_2O_3 is incorporated. However, it is clear that the experimental lattice thermal conductivity of the composite materials is significantly lower than the predicted from EMT, reaching the value of $7.1 W/m{\cdot}K$. Therefore, the higher predicted values from "EMT ($CoSi/Al_2O_3$)" compare to the experimental data suggest the contribution of an additional phase.

Moreover, the effect of the porosity on the reduction of the lattice thermal conductivity in these materials cannot be excluded. Thus, in this case $(\mathrm{CoSi}/\mathrm{Al_2O_3}/\mathrm{Pores})$, the Equation (4) was written as

$$f_1 \frac{\kappa_1 - \kappa}{\kappa_1 + 2\kappa} + f_2 \frac{\kappa_2 - \kappa}{\kappa_2 + 2\kappa} + f_3 \frac{\kappa_3 - \kappa}{\kappa_3 + 2\kappa} = 0 \text{ and } f_1 + f_2 + f_3 = 1, \quad (5)$$

where f_1, f_2, and f_3 are the fractions of the matrix phase, the nano-phase and the porosity, respectively, and κ_1, κ_2, and κ_3 are the lattice thermal conductivities of the same phases. The fractions f_1 and f_2 were known while f_3 is taken from Table 1. Then, by taking into consideration the known volume fractions, the thermal conductivity of the matrix $(\kappa_1 = 13.38\mathrm{W/m{\cdot}K})$, the thermal conductivity of the $\mathrm{Al_2O_3}$ $(\kappa_2 = 16\mathrm{W/m{\cdot}K})$, as well as the thermal conductivity of the air $(\kappa_3 = 0.0256\mathrm{W/m{\cdot}K})$, Equation (5) is solved numerically for "κ". The results of such calculations are shown in Figure 6 labelled "EMT$(\mathrm{CoSi}/\mathrm{Al_2O_3}/\mathrm{Pores})$". According to the calculations the lattice thermal conductivity was predicted to reduce from 12.3W/m·K to about 10.1W/m·K when 15% $\mathrm{Al_2O_3}$ is incorporated. However, it is clear that the experimental lattice thermal conductivity of the composite materials is still significantly lower than the predicted from EMT reaching the value of 7.1W/m·K, which is a significant difference. Such difference can be attributed to the existence of $\mathrm{Al_2O_3}$ at nanoscale while EMT concerns composites with constituent phases at macro- or micro-scale.

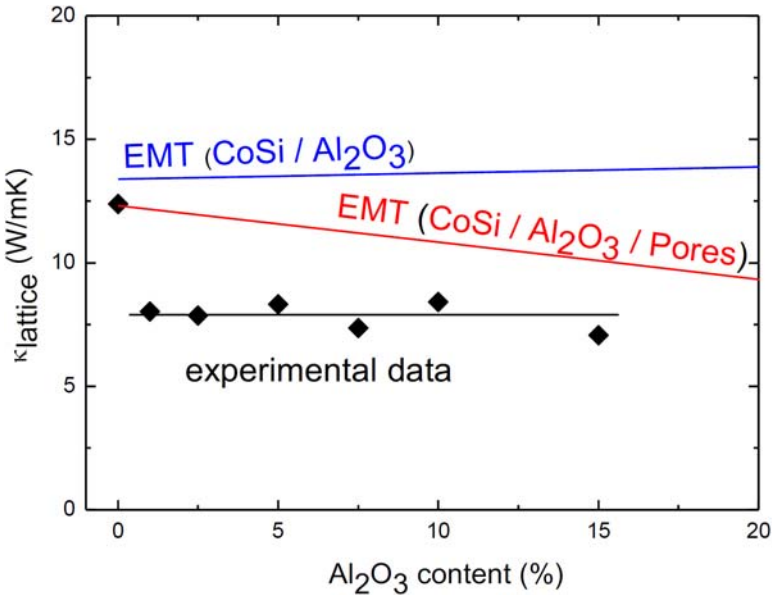

Figure 6. Room temperature lattice thermal conductivity by "effective medium theory (EMT)" of the hot-pressed (1-x) CoSi /x Al_2O_3 nanocomposites pellets as a function of the Al_2O_3 content.

4. Conclusion

In conclusion, CoSi/x Al_2O_3 nanocomposites materials have been synthesized by using CoSi as matrix and nano-Al_2O_3 via solid state reaction, mechanical mixing, and hot pressing. Seebeck coefficient was found to be similar for all samples suggesting similar doping level as expected. On the other hand, the electrical conductivity was significantly decreased and this is attributed to the existence of Al_2O_3 on the grain boundaries of the pellets. The thermal conductivity was initially found to decrease and then remained constant with increasing Al_2O_3 concentration. The reduction of lattice thermal conductivity via the formation of nanocomposite materials was discussed in the view of effective medium theory based on two different cases considering

$CoSi/Al_2O_3$ and $CoSi/Al_2O_3/Pores$ contributions. The experimental data were closer to the $CoSi/Al_2O_3/Pores$ model, although still lower than predicted. This difference can be attributed to the nano-effect of Al_2O_3 while such process is useful for the optimization of thermoelectric materials. More work can be done on the development of nanocomposites with less aggregates where more nano-phase contributes in the thermoelectric properties.

Acknowledgements

This work is part of the Si-THERM Project supported by the Cyprus Research Promotion Foundation's Framework Programme for Research, Technological Development and Innovation 2009-2010 (DESMI 2009-2010), co-funded by the Republic of Cyprus and the European Regional Development Fund and specially under grant PEEK/0311/07. EDX mapping was done on equipment supported by funding from the European Regional Development Fund and the Republic of Cyprus, through the Research Promotion Foundation (Project normal/0308/17).

References

[1] S. Asanabe, D. Shinoda and Y. Saski, Phys. Rev. A 134 (1964), 774.

[2] G. T. Alekseeve, V. K. Zailsev, A. V. Petrov, V. I. Tarasov and M. I. Fedorov, Sov. Phys. Solid State 23 (1981), 1685.

[3] S. W. Kim, Y. Mishima and D. C. Choi, Intermetallics 10 (2002), 177.

[4] K. Maex and M. V. Rossum, Properties of Metal Silicides, INSPEC Institute of Engineers, London, 1995.

[5] W. L. Ren, C. C. Li, L. T. Zhang, K. Ito and J. S. Wu, J. All. Compds. 392 (2005), 50.

[6] E. Skoug, C. Zhou, Y. Pei and D. T. Morelli, Appl. Phys. Lett. 94 (2009), 022115.

[7] R. R. Heikes and R. W. Ure, Thermoelectricity: Scien. and Engin., New York, Interscience 427 (1961).

[8] S. F. Fan, J. N. Zhao, Q. Y. Yan, J. Ma and H. H. Hng, J. Electron. Mater. 40 (2011), 1018.

[9] H. Lu, P. G. Burke, A. C. Gossard, G. Zeng, A. T. Ramu and J. H. Bahk et al., Adv. Mater. 23 (2011), 2377.

[10] D. H. Park, M. Y. Kim and T. S. Oh, Curr. Appl. Phys. 11 (2011), S41.

[11] V. A. Kulbachinskii, V. G. Kytin, M. Y. Popov, S. G. Buga, P. B. Stepanov and V. D. Blank, J. Solid State Chem. 193 (2012), 64.

[12] M. Y. Kim, B. K. Yu and T. S. Oh, Electron. Mater. Lett. 8 (2012), 269.

[13] W. J. Xie, J. He, H. J. Kang, X. F. Tang, S. Zhu and M. Laver et al., Nano Lett. 10 (2010), 3283.

[14] E. Alleno, L. Chen, C. Chubilleau, B. Lenoir, O. Rouleau and M. F. Trichet et al., J. Electron. Mater. 39 (2010), 1966.

[15] M. K. Keshavarz, D. Vasilevskiy, R. A. Masut and S. Turenne, J. Electron. Mater. 42 (2013), 1429.

[16] J. L. Mi, X. B. Zhao, T. J. Zhu and J. P. Tu, Appl. Phys. Lett. 91 (2007).

[17] M. Ioannou, E. Symeou, J. Giapintzakis and Th. Kyratsi, J. Electron. Mater. 43 (2014), 3824.

[18] G. T. Alekseeva, V. K. Zaitsev, A. V. Petrov, V. I. Tarasov and M. I. Fedorov, Sov. Phys. Solid State 23 (1981), 1685.

[19] V. K. Zaitsev, M. I. Fedorov, V. I. Tarasov and A. Adilbekov, Sov. Phys. Solid State 19 (1976), 996.

[20] V. K. Zaitsev, M. I. Fedorov, S. V. Ordin and V. I. Tarasov, Sov. Phys. Solid State 20 (1978), 890.

[21] V. I. Odelevskii, J. Tech. Phys. 21 (1953), 667.

[22] R. J. Landauer, Appl. Phys. 23 (1952), 779.

[23] James F. Shackelford and Robert H. Doremus (Editors), Ceramic and Glass Materals: Structure, Properties and Processing, 2008.

■